Investigating the Effects of Upper Lapse Rate and Surface Heat Flux on an idealized Convective Atmospheric Boundary Layer Entrainment Layer using Large Eddy Simulation

by

Niamh Chaparro

A THESIS SUBMITTED IN PARTIAL FULFILLMENT
OF THE REQUIREMENTS FOR THE DEGREE OF

MSc

in

THE FACULTY OF GRADUATE STUDIES
(Earth, Ocean and Atmospheric Sciences)

The University Of British Columbia
(Vancouver)

missing submission month *missing submission year*

Table of Contents

1. Results in Context

1.1 Comparison of general Set-up

Sullivan and Patton (2011) found that the shapes of the average potential temperature ($\overline{\theta}$) and average vertical heat flux ($\overline{w'\theta'}$) profiles, as well as the measured **CBL!** height vary depending on grid size. The resolution at which convergence begins is listed in Table 1.1. At lower resolution the $\overline{\theta}$ and $\overline{w'\theta'}$ profiles are such that the **EL!** is a larger portion of the **CBL!** and measured **CBL!** height is higher. Overall they concluded that vertical resolution was more critical. This compliments the conclusion Brooks and Fowler (2012) reached when discussing their resolution test. That is, to capture the steep vertical gradients in the **EL!** requires high vertical resolution.

As Turner discusses in his 1986 review of turbulent entrainment, smaller scale processes, such as those at the molecular level are relatively unimportant. Large scale engulfment and trapping between thermals dominates. If $\overline{\theta'^2}$ is calculated based on differences from horizontally averaged θ, applying the ergodic assumption, then it is a measure of horizontal variance at a point in time. Although Sullivan and Patton (2011) found that the vertical distance over which $\overline{\theta'^2}$ varied significantly more or less converged at the resolution shown in Table 1.1 the maximum continued to increaase up to their finest grid spacing (5, 5, 2).

The question as to whether mixing and gradients within the **EZ!** are adequately resolved serves as motivation for **DNS!** studies such as that of Gar-

Table 1.1: Grid spacing around the **EL!** used in comparable **LES!** studies. Those used for resolution tests are not listed here. For Sullivan and Patton's 2011 resolution study I list the grid sizes at which profiles within the **EL!** and **CBL!** height evolution began to converge.

Publication	Δx, Δy, Δz	Horizonal
Publication	in the **EZ!** (m)	Domain (km^2)
Sullivan et al. (1998)	33, 33, 10	5 x 5
Federovich et al. (2004)	100, 100, 20	5 x 5
Brooks and Fowler (2012)	50, 50, 12	5 x 5
Sullivan and Patton (2011)	20, 20, 8	5 x 5
This study	25, 25, 5	3.4 x 4.8

cia and Mellado (2014). These authors found the entrainment ratio $\frac{\overline{w'\theta'}_{z_f}}{\overline{w'\theta'}_s}$ to be about 0.1 which is lower than for example what Federovich et al. (2004) observed, but close to what was seen in Figures **??** and **??**. Based on their $\overline{w'\theta'}$ profiles the depth of the region of negative flux is comparable to what's shown in Figure **??**. Furthermore, these author's concluded that the production and destruction rates of **TKE!**, as well as the entrainment ratio used to calculate the entrainment rate, were effectively independent of molecular scale processes.

The **FFT!** energy spectra of the turbulent velocities at the top of the **ML!** show a substantial resolved intertial subrange giving confidence in the choice of horizontal grid size used. In the **EZ!** where turbulence is intermittent, the dominant energy containing structures are smaller, and decay to the smallest resolved turbulent structures is steeper. This confirms the assertion of Garcia and Mellado (2014) that the **EZ!** is separated into two sublayers in terms of turbulence scales.

The horizontal domain in this study is relatively small (see Table 1.1). However, visualizations of horizontal and vertical slices clearly showed multiple

resolved thermals with diameter increasing with increased **CBL!** height, but remaining less than or on the order of 100 meters. Sullivan et al. (1998) carried out one run on a smaller domain with higher resolution, noticed it resulted in lower **CBL!** height and concluded this was due to restricted plume size. However, given the results of Sullivan and Patton (2011) it could have been an effect of the grid size.

Brooks and Fowler (2012) encountered significant scatter when basing heights of average profiles. Sullivan et al. (1998)'s heights based on average profiles produced very jagged oscillating timeseries. But the heights based on average profiles here, using an ensemble of cases, varied smoothly in time. This could be attributed to a smoother profile based on a greater number horizontal points (10*128*192).

The principle parameter describing the balance of forces in idealized **CBL!** entrainment is the Richardson number **Ri!** and its magnitude depends on the way in which the θ jump is defined. Varying this can cause identical conditions can be described by quite different $acsRi$ s. The **Ri!** range in this study was dependent on variation in γ and less so on $\overline{w'\theta'}_s$. Brooks and Fowler (2012) and Sullivan et al. (1998) imposed a θ jump of varying strength topped by a constant γ. Whereas Federovich et al. (2004) initialized with a constant heat flux, with a layer of uniform θ, topped by a constant γ. They varied γ and kept $\overline{w'\theta'}_s$ constant for each run. Their range of γ, definitions of the θ jump and **Ri!** range are directly comparable to those of this study, whereas those of Brooks and Fowler (2012) and Sullivan et al. (1998) are quite different. The θ jumps defined in these sudies were smaller.

1.2 Local ML! Heights

Sullivan et al. (1998) determined local **CBL!** height by locating the point of maximum gradient. Analysis of the resulting distributions showed dependence of standard deviation and skewness on Richardson number. The

Table 1.2: Initial conditions used in comparable **LES!** studies.

Publication	$\overline{w'\theta'}_s$ W/m^2	γ K/km	Initial θ Jump K	**Ri!** range
Sullivan et al. (1998)	20 - 450	3	.436 - 5.17	1 - 100
Federovich et al. (2004)	300	1 - 10	na	10 - 40
Brooks and Fowler (2012)	10 -100	3	1 - 10	10 - 100
This study	60 - 150	2.5 - 10	na	10 - 30

normalized standard deviation decreased with increased **Ri!** whereas skewness was alomost bimodal; being negative at high **Ri!** and positive and low **Ri!**. Iniatially in this study, I applied a similar method and found distributions with lower **Ri!** to have positive skew. Upon exhaustive inspection of local vertical θ profiles, it became evident that at certain horizontal points high gradients well into the free atmposphere exceded those closer to the location of the **CBL!** height reasonably identified by eye.

Locating the **ML!** height using the multi-linear regression method employed proved more reliable. The resulting distributions, normalized by h showed a decrease in the lowest $\frac{h_0^l}{h}$ resulting in an apparant increased negative skew with decreasing stability (decreasing **Ri!**). This combined with an increase in spread agrees with the findings Sullivan et al. (1998) and supports the results of **??**. The approximate scaled **EZ!** based on the $\frac{h_0^l}{h}$ distributions is about 0.2 - 0.4 whereas that based on distributions of local maximum tracer gradients by Brooks and Fowler (2012) was smaller (.05 - .2). But the local maximum gradient of the tracer profile would likely be within the **EZ!** at points outside an actively impinging plume and so higher than the **ML!** top (h_0^l) defined here.

As expected, with increased $\overline{w'\theta'}_s$ the variance and magnitude of the vertical velocity fluctuations within and at the limits of the **EZ!** increase. Greater turbulent velocity causes results in a higher **CBL!** and a thicker **EZ!** over

which warmer air from higher up is brought down and relatively cooler air from below is brought up. So the magnitude and spread of $\theta^{'}$ increases. All of this agrees with the findings of Sorbjan (1996), but the portion of the $\frac{w^{'}}{w^{*}}$ distribution where $\theta^{'}$ is positive appears to narrow as γ increases. This contradicts his assertion that velocities are uninfluenced by this parameter while the effectiveness of w^{*} as a scale for $w^{'-}$ where $\theta^{'} > 0$ supports it.

Although the motion of the thermals dominates the dynamics witin the **EZ!**, the $w^{'-}\theta^{'-}$, $w^{'+}\theta^{'-}$ and $w^{'-}\theta^{'+}$ quadrants do approximately cancel as Sullivan et al. (1998) concluded. The downward moving warm quadrant ($w^{'-}\theta^{'+}$) for example, at h, represents warmer free atmosphere air that is being entrained. So it's magnitude at a certain point in time is an indication of how much the region below will be warmed due to entrainment at a successive time. The increase of $\overline{w^{'-}\theta^{'+}}_h$ in time is primarily due to $\theta^{'+}$ which is effectively scaled by the temperature scale $(h_1 - h)\gamma$. A very similar scale was introduced by Garcia and Mellado ([4]) to further their line of reasoning that the buoyancy in the upper **EZ!** is determined by γ. Figure 1.1 illustrates a broad qualitative explaination for its effectiveness. At h much of the air is at the background (or initial) potential temperature $\overline{\theta}_0(h)$, but some air of $\theta = \overline{\theta}_0(h_1)$ is brought down from h_1 resulting in positive temperature fluctuations at h ($\theta^{'+}$).

Garcia and Mellado ([4]) suggest that the buoyancy in the lower portion of the **EZ!** ie from a point just below h down is more influenced by the vigourous turbulence of the **ML!** so mixing reduces the difference between the temperature at the top of the **ML!** and that at or just below h. However, the observation in Section **??** that the magnitude of the vertical potential temperature gradient in the upper **ML!** increases with increasing γ indicates that the influence of this parameter extends further. Related, is the increased magnitude of the minimum $\overline{w^{'}\theta^{'}}$ with γ, seen here and in both Sorbjan's (1996) and FedConzMir04 (2004), which leads to an increased $-\frac{\partial \overline{w^{'}\theta^{'}}}{\partial z}$ in the lower **EZ!** and so increased warming per Equation **??**.

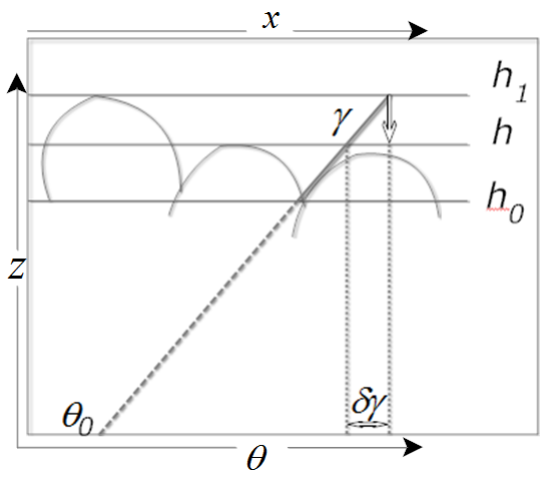

Figure 1.1: Illustration of the potential temperature scale $(h_1 - h)\gamma = \delta\gamma$: The curves represent vertical a cross-section of thermal tops. Between them is stable air at the initial lapse rate γ. h_1, h correspond to the highest and average thermal height respectively and h_0 is the top of the well mixed region (**ML!**). The initial temperature is $\theta_0 = \overline{\theta}_0$. A thermal will initiate the downward movement of air from h_1 to h, and the difference between its potential temperature and that of the background stable air at h is $(h_1 - h)\gamma = \delta\gamma$.

$$\frac{\partial \overline{\theta}}{\partial t} = -\frac{\partial}{\partial z}\overline{w'\theta'} \tag{A.21}$$

1.2.1 Relationship of Entrainment Layer Depth to Richardson Number

The **EZ!** is inhomogenous and on average is a region of transition as clearly represented by the $\overline{\theta}$ profile. It's where relatively cooler thermals overturn or recoil initiating entrainment as represented by the heat flux profile. The $\overline{\theta}$ profile partially characterizes the thermodynamic state of the **CBL!** as well defining its three layer structure. It is directly comparable to both bulk models and local θ profiles which in turn are comparable to a sounding, unlike a heat flux profile which is an inherently average quantity.

Neither of the two comparable **LES!** (see Table **??**) studies define the **EL!** based on the vertical $\frac{\partial\overline{\theta}}{\partial z}$ profile. So, to enable direct comparison heights were based on the heat flux profile. In this framework Federovich et al.'s (2004) show decreasing scaled **EZ!** with increaseing **Ri !** (decreasing **Ri!**$^{-1}$) and conclude an exponent of of $-\frac{1}{2}$. They attribute the decrease in the overall depth to a slight decrease in the scaled top limit over time. However based on their plot, it seems to go from about 0.5 to 0.2.

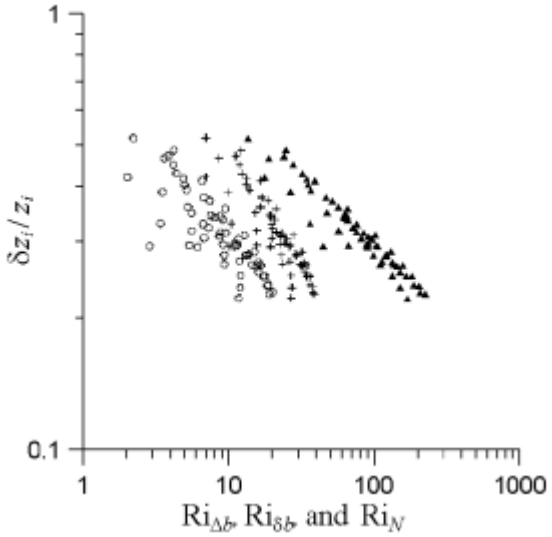

Figure 1.2: Figure 9 from Federovich et al.'s (2004) representing Equation **??** using three different Richardson numbers, in log-log coordinates. $Ri_{\Delta b}$ (circles) and $Ri_{\delta b}$ (crosses) correspond directly to those determined here using $\delta\theta$ and $\Delta\theta$ based on the heat flux profiles. Note their Δ refers to the smaller θ jump, ie that at z_f, whereas I use it for the larger. Then Ri_N (triangles) is the Richardson number defined in Equation **??**, with w^* and z_f as the velocity and length scale.

Brooks and Fowler (2012) found no clear **Ri!** dependence of the scaled **EL!** depth based on the heat flux profle, but their definition was based on the lower part $(z_{f1} - z_f)$. According to Federovich et al. (2004) this lower sub-

layer does not vary in time. Figure **??** shows that when based on the heat flux profiles as Federovich et al.'s (2004) did, there is no clear dependence on **Ri!**. This is supported by the similarity in time and accross runs of the vertical turbulent heat flux profiles when scaled by $(\overline{w'\theta'})_s$.

The most obvious possible cause for this disagreement is the difference in grid size shown in Table 1.1. Inspection of their heat flux profiles confirms a relatively deeper region of negative flux as compared with those seen here (.4 vs .25). Their surface heat flux was twice the highest used here, but their range of **Ri!** is comparable to that of this study. This latter point although not directly relevent here, serves as confirmation that γ is the more influential parameter.

Publication	**EZ!** Depth	**CBL!** height	θ Jump
Federovich et al. (2004)	$z_{f1} - z_{f0}$	z_f	$\overline{\theta}(z_{f1}) - \overline{\theta}(z_{f0})$
Brooks and Fowler (2012)	$2\times(z_f - z_{f0})$	z_f	average of local values

Here, when heights are defined on the scaled vertical potential temperature gradient profile $\frac{\frac{\partial\overline{\theta}}{\partial z}}{\gamma}$ the curve representing Equation **??**

$$\frac{\Delta h}{h} \propto Ri^b \tag{??}$$

and show an (or slope) exponent b which increases in magnitude from about $-\frac{1}{2}$, as predicted and seen by Boers (1989), to about -1 as justified in Nelson et al. (1989), with increasing **Ri!** (decreasing $\mathbf{Ri!}^{-1}$). Overall there is a clear narrowing of the scaled **EZ!** depth with increased **Ri!** (decreased $\mathbf{Ri!}^{-1}$) as indicated by the local height distributions in Section **??**. Although based on different height definitions Federovich et al. (2004) concluded an exponent $b = -\frac{1}{2}$ and Brooks and Fowler's (2012) plots show curves with an apparant

exponent less in magnitude than -1.

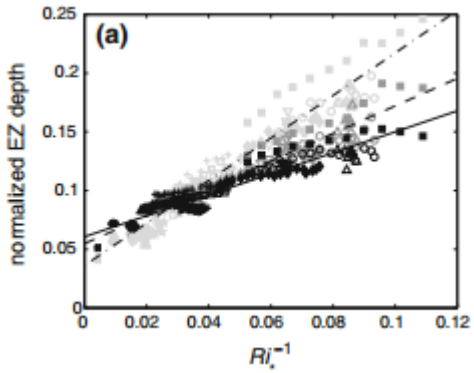

Figure 1.3: This is panel (a) from Figure 5 in Brooks and Fowler's (2012) and represents relationship **??**. Heights are based on the distributions of local maximum tracer gradients, ie upper and lower percentiles. Their θ jump is an average of the potential temperature differences accross the regions of significant wavelet covariance in the local tracer profiles.

The curves in Figure 1.3 seem to separate out for each run. In this study, before scaling the $\frac{\partial \overline{\theta}}{\partial z}$ profile curves in Figure **??** separate out, but in the reverse order. Runs under higher stability have larger scaled **EZ!** dephts. Brooks and Fowler (2012)'s runs with initially lower **Ri!** (higher $\mathbf{Ri!}^{-1}$) have larger scaled **EZ!** depths than runs with initially higher **Ri!**s, even where **Ri!** values overlap.

Neither study addresses a change in exponent with increased **Ri!**. It is possible that there is a change in entrainment mechanism. Sullivan et al. (1998) observed enfolding and engulfment at lower **Ri!**. Whereas at higher **Ri!** when motion is more restricted, entraiment seemed to occur via trapping of thinner whisps at the edge of an upward moving thermal. Turner (1986) also distiguishes between entrainment by convective overturning and recoil. Garcia and Mellado's (2014) refer to a change in entrainment rate due to the effects of increased stability on the upper **EZ!** sublayer. In this study, although the narrowing of the **EZ!** as defined here depends predominantly

on the magnitude of the potential temperature gradient in the lower **EZ!** and upper **ML!** the scaled magnitude of upper limit based on the $\frac{\partial\overline{\theta}}{\partial z}$ does appear to decrease slightly in time. So this could correspond to the mention of a slowly decreasing upper sub layer in the **EZ!** in both Garcia and Mellado (2014) and Federovich et al. (2004).

1.3 Relationship of Entrainment Rate to Richardson Number (Q3)

The magnitudes of **Ri!** numbers determined in this and the comparable studies are primarily influenced by the magnitude of the θ jump. So with different definitions you can have the same conditions represented by a different **Ri!** value. Here, I define it in two ways as both Federovich et al. (2004) and Garcia and Mellado (2014) did. I do this based on the flux profile for the purpose of direct comparison with these studies and to observe how the change in definition effects Equation **??**.

$$\frac{w_e}{w^*} \propto Ri^a \tag{??}$$

As in these studies, the larger jump ie that taken accross the **EZ!** ($\Delta\theta$) yields a larger a as Federovich et al. (2004) conclude. Although Garcia and Mellado (2014) interpret their curves as both asymptoting to a straight line ($a = -1$) as the upper **EZ!** sublayer narrows. Based on their plots alone, ie in the absence of their justification based on the derivation of the entrainment relation, I would not conclude this asymtotic behavior. Rather for $Delta\theta$ I see a curve with increasing exponent exceeding magnitude -1 at higher **Ri!**. For $\delta\theta$ I see a curve with exponent less in magnitude than -1.

That there is an analogous distinction between plots of Equation **??** using $\Delta\theta$ vs $\delta\theta$ when all heights are defined on the $\frac{\frac{\partial\overline{\theta}}{\partial z}}{\gamma}$ profile lends some credence to this framework. Scatter is least when the θ jump is defined accross the

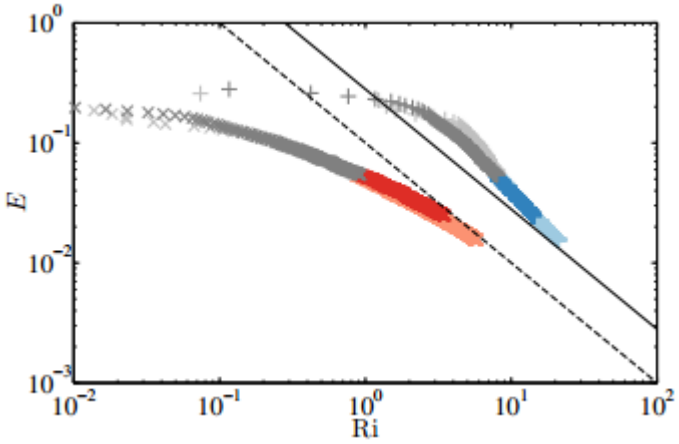

Figure 1.4: This is Figure 11 from Garcia and Mellado (2014) and represents equation **??** based on the two θ jumps. The grey and blue curve is based on $\Delta\theta$ and the red curve is based on something similar to $\delta\theta$, ie $\overline{\theta}(h) - \overline{\theta}_0(h)$. The dashed and continuous black lines represent the straight lines two which the curves asymptote according to their analysis. Their defined heights are comparable to those based on the heat flux profile in Figure **??**.

EL!. In this plot $-\frac{3}{2}$ fits at higher **Ri!** (lower **Ri!**$^{-1}$) and -1 seems to fit at lower **Ri!**. Combined with the apparant change in b for Equation **??** this could be interpreted as an indication of a change in entrainment regime at increased **Ri!**.

1.4 Conclusion

The magnitude and variance of local height increase with increasing $\overline{w'\theta'}_s$ and decrease with increasing γ. Similarly for the vertical velocity fluctuations in the **EZ!**. However increased γ results in an increase in the positive temperature fluctuations at h. The magnitude of these positive temperature perturbations at points where vertical velocity is negative represents downward moving entrained air. Below h in the lower **EZ!** the temperature gradient increases with increasing γ. So, the growth of the idealized dry

CBL! is driven by $\overline{w'\theta'}_s$ and suppressed by γ. But warming is due to $\overline{w'\theta'}_s$ and the entrainment of air from aloft the temperature of which in turn depends on γ.

Both the **EZ!** depth and **CBL!** height based on the average $\frac{\frac{\partial\overline{\theta}}{\partial z}}{\gamma}$ profile show dependence on **Ri!** as seen in other studies and justified theoretically. This profile serves to characterize the **CBL!** and links bulk models to soundings via an **LES!**. So it is a valid way of defining the **CBL!** and its **EZ!**. Plots of Equations exhibit changes in exponent. A change in entrainment mechanism or regime with increased **Ri!** has been observed in measurement as well as **LES!** and justified theoretically. I suggest the change in exponents represent this.

Throughout this study threads the influence of γ. The convecive time scale $\tau = \frac{w^*}{h}$ and **Ri!** group according to this parameter. This justifies the use of the brunt vaisalla time scale as well as the constant heat flux with varying lapse rate of Federovich et al. (2004). I conclude once the effects of $\overline{w'\theta'}_s$ are accounted for through h, γ remains the dominant parameter in idealized **CBL!** entrainment.

References

Boers, R., 1989: A parametrization of the depth of the entrainment zone. *Journal of Applied Meteorology*, 107–111.

Brooks, I. M. and A. M. Fowler, 2012: An evaluation of boundary-layer depth, inversion and entrainment parameters by large-eddy simulation. *Bundary-Layer Meteorology*, **142**, 245–263.

Federovich, E., R. Conzemus, and D. Mironov, 2004: Convective entrainmnent into a shear-free, linearly stratifies atmosphere: Bulk models reevaluated through large eddie simulation. *Journal of the Atmospheric Sciences*, **61**, 281 – 295.

Garcia, J. R. and J. P. Mellado, 2014: The two-layer structure of the entrainment zone in the convective boundary layer. *Journal of the Atmospheric Sciences*, doi:10.1175/JAS-D-130148.1.

Nelson, E., R. Stull, and E. Eloranta, 1989: A prognostic relationship for entrainment zone thickness. *Journal of Applied Meteorology*, **28**, 885–901.

Sorbjan, Z., 1996: Effects caused by varying the strenth of the capping inversion based on a large eddie simulation of the shear free convective boundary layer. *Journal of the Atmospheric Sciences*, **53**, 2015 – 2023.

Sullivan, P. P., C.-H. Moeng, B. Stevens, D. H. Lenschow, and S. D. Mayor, 1998: Structure of the entrainment zone capping the convective atmospheric boundary layer. *Journal of the Atmospheric Sciences*, **55**, 3042–3063, doi:10.1007/s10546-011-9668-3.

Sullivan, P. P. and E. G. Patton, 2011: The effect of mesh resolution on convective boundary layer statistics and structures generated by large eddie simulation. *Journal of the Atmospheric Sciences*, **58**, 2395–2415, doi:10.1175/JAS-D-10-05010.1.

Turner, J. S., 1986: Turbulent entrainment: the development of the entrainment assumption and its application to geophysical flows. *J. Fluid Mech.*, **173**, 431–471.

A. Appendices

A.1 Potential Temperature: θ

$$\theta = T\left(\frac{p_0}{p}\right)^{\frac{R_d}{c_p}} \tag{A.1}$$

p_0 and P are a reference pressure and pressure respectively.

$$\frac{c_p}{\theta}\frac{d\theta}{dt} = \frac{c_p}{T}\frac{dT}{dt} - \frac{R_d}{p}\frac{dp}{dt} \tag{A.2}$$

If changes in pressure are negligible compared to overall pressure, as in the case of that part atmosphere that extends from the surface to 2Km above it.

$$c_p\frac{d\theta}{\theta} = c_p\frac{dT}{T} - \frac{R_d}{p}\frac{dp}{p} \tag{A.3}$$

$$\frac{d\theta}{\theta} = \frac{dT}{T} \tag{A.4}$$

and if

$$\frac{\theta}{T} \approx 1 \tag{A.5}$$

then small changes in temperature are approximated by small changes in potential temperature

$$d\theta \approx dT \; or \; \theta^{'} \approx T^{'} \tag{A.6}$$

and at constant pressure change in enthalpy (H) is

$$dH = c_p dT. \tag{A.7}$$

A.2 Second Law of Thermodynamics

$$\frac{ds}{dt} \geq \frac{q}{T} \tag{A.8}$$

For a reversible process

$$\frac{ds}{dt} = \frac{q}{T} \tag{A.9}$$

Using the first law and the equation of state for an ideal gas

$$\frac{q}{T} = \frac{1}{T}\left(\frac{dh}{dt} - \alpha\frac{dp}{dt}\right) = \frac{c_p}{T}\frac{dT}{dt} - \frac{R_d}{p}\frac{dp}{dt} \tag{A.10}$$

so

$$\frac{ds}{dt} = \frac{q}{T} = \frac{c_p}{\theta}\frac{d\theta}{dt} \tag{A.11}$$

For a dry adiabatic atmosphere

$$\frac{ds}{dt} = \frac{c_p}{\theta}\frac{d\theta}{dt} = 0 \tag{A.12}$$

A.3 Reynolds Decomposition and Simplification of Conservation of Enthalpy (or Entropy) for a dry Atmosphere

$$\frac{\partial\theta}{\partial t} + u_i\frac{\partial\theta}{\partial x_i} = \nu_\theta\frac{\partial^2\theta}{\partial x_i^2} - \frac{1}{c_p}\frac{\partial Q^*}{\partial x_i} \tag{A.13}$$

ν and Q^* are the thermal diffusivity and net radiation respectively. If we ignore these two effects then (adiabatic?)

$$\frac{\partial\theta}{\partial t} + u_i\frac{\partial\theta}{\partial x_i} = 0 \tag{A.14}$$

$$\theta = \overline{\theta} + \theta^{'}, \theta = \overline{u_i} + u_i^{'} \tag{A.15}$$

$$\frac{\partial \overline{\theta}}{\partial t} + \frac{\partial \theta^{'}}{\partial t} + \overline{u_i}\frac{\partial \overline{\theta}}{\partial x_i} + u_i^{'}\frac{\partial \overline{\theta}}{\partial x_i} + \overline{u_i}\frac{\partial \theta^{'}}{\partial x_i} + u_i^{'}\frac{\partial \theta^{'}}{\partial x_i} = 0 \tag{A.16}$$

Averaging and getting rid of average variances and their linear products

$$\frac{\partial \overline{\theta}}{\partial t} + \overline{u_i}\frac{\partial \overline{\theta}}{\partial x_i} + u_i^{'}\frac{\partial \theta^{'}}{\partial x_i} = 0 \tag{A.17}$$

Ignoring mean winds

$$\frac{\partial \overline{\theta}}{\partial t} + u_i^{'}\frac{\partial \theta^{'}}{\partial x_i} = 0 \tag{A.18}$$

using flux form

$$\frac{\partial \overline{\theta}}{\partial t} + \frac{\partial (u_i^{'}\theta^{'})}{\partial x_i} - \theta^{'}\frac{\partial u_i^{'}}{\partial x_i} = 0 \tag{A.19}$$

under the bousinesq assumption $\Delta \dot{u}_i = 0$

$$\frac{\partial \overline{\theta}}{\partial t} = -\frac{\partial (u_i^{'}\theta^{'})}{\partial z} \tag{A.20}$$

ignoring horizontal fluxes

$$\frac{\partial \overline{\theta}}{\partial t} = -\frac{\partial (w^{'}\theta^{'})}{\partial z} \tag{A.21}$$

A.4 Reynolds averaged Turbulence Kinetic Energy Equation

$$\frac{\partial \overline{e}}{\partial t} + \overline{U}_j\frac{\partial \overline{e}}{\partial x_j} = \delta_{i3}\frac{g}{\overline{\theta}}\left(\overline{u_i^{'}\theta^{'}}\right) - \overline{u_i^{'}u_j^{'}}\frac{\partial \overline{U}_i}{\partial x_j} - \frac{\partial\left(\overline{u_j^{'}e^{'}}\right)}{\partial x_j} - \frac{1}{\overline{\rho}}\frac{\partial\left(\overline{u_i^{'}p^{'}}\right)}{\partial x_i} - \epsilon \tag{A.22}$$

e is turbulence kinetic energy (TKE). p is pressure. ρ is density. ϵ is viscous dissipation.